European Journal of Pharmaceutical Sciences 212 (2025) 107183

Contents lists available at ScienceDirect

European Journal of Pharmaceutical Sciences

journal homepage: www.elsevier.com/locate/ejps

Advancing continuous encapsulation and purification of mRNA vaccines and therapeutics

Ehsan Nourafkan [a,b], Zidi Yang [b], Mabrouka Maamra [b], Zoltán Kis [b,c,*]

[a] Department of Biochemical Engineering, University College London, Marshgate Building, London E20 2AE, UK
[b] School of Chemical, Materials and Biological Engineering, University of Sheffield, Mappin Street, Sheffield S1 3JD, UK
[c] Department of Chemical Engineering, Imperial College London, Roderic Hill Building, South Kensington Campus, London SW7 2AZ, UK

ARTICLE INFO

Keywords:
Continuous manufacturing
mRNA
Microfluidic mixing
Lipid nanoparticles
Real-time in-line monitoring
Tangential flow filtration

ABSTRACT

The messenger RNA (mRNA) platform technology is advancing the deployment of vaccines and therapeutics to combat various diseases. The COVID-19 pandemic highlighted the urgent need for large-scale mRNA vaccine production, exposing supply constraints and driving demand for more cost-effective and scalable manufacturing solutions. To address these challenges, integrated and continuous mRNA manufacturing processes provide significant advantages over traditional batch methods, including increased efficiency, reduced labor requirements, a smaller manufacturing footprint, and faster production. Here, we present the first continuous process integrating: 1) continuous flow encapsulation of mRNA into lipid nanoparticles (LNPs), 2) real-time in-line particle size and polydispersity index (PDI) monitoring using spatially-resolved dynamic light scattering, 3) single-pass tangential flow filtration (SP-TFF) purification of mRNA-LNPs. The continuously produced and SP-TFF purified mRNA-LNP critical quality attributes are: 95.5 ± 4 % encapsulation efficiency, 105±6 nm average particle size, 0.1 ± 0.02 PDI, 0.003 % residual ethanol content, 0.4 ± 0.05 % fraction of unloaded LNPs, 86.2 ± 3 % mRNA integrity, and the final pH of 7. During the TFF purification, an increase in average mRNA-LNP size and formation of bleb compartments on the particle's surface was also observed. Additionally, a 90 % recovery of mRNA-LNPs was achieved using regenerated cellulose (RC) membrane SP-TFF with an overall concentration factor of 10X. This study lays the foundations for faster and more efficient manufacturing of high-quality mRNA vaccines and therapeutics.

1. Introduction

In recent years, mRNA-based vaccines and therapeutic candidates have been emerging for the treatment of a wide range of diseases (e.g. genetic, inflammatory, infectious, and cancer) (Qin et al., 2022; Wang et al., 2023; Zhang et al., 2023). The mRNA vaccine and therapeutic production process includes two main phases: 1-mRNA drug substance (mRNA-DS) and 2-mRNA drug product (mRNA-DP) manufacturing (Fig. 1) (Webb et al., 2022). The mRNA technology is increasingly recognized as a leading platform for vaccine and therapeutics development, with potential applications in infectious diseases, cancer immunotherapy, and genetic disorders (Wang et al., 2023; Zhang et al., 2023; Maxmen, 2024; Webb et al., 2022).

The mRNA technology played a pivotal role during the COVID-19 pandemic, enabling the rapid development of SARS-CoV-2 vaccines. However, the global demand for these vaccines outpaced supply capabilities, primarily due to manufacturing bottlenecks. To address these challenges and meet growing future vaccine and therapeutic demands, intensifying the mRNA production process through a closed, continuous, multi-product platform has emerged as a promising solution. Such platforms can leverage single-use components and advanced process analytics (in-line, on-line, and at-line) to increase manufacturing productivity (Gerstweiler et al., 2021). An integrated and continuous manufacturing platform offers four key advantages over traditional batch manufacturing. First, the productivity, expressed as the amount of product generated per unit time and per unit process scale, is substantially higher in continuous compared to batch processing. Second, efficiency is greater in continuous production due to minimized waste and fewer quality inconsistencies during start-up and shut-down phases, which represent a larger fraction of total runtime in batch processes than in continuous ones. Third, as a result of higher productivity and efficiency, the process scale and facility footprint required for a given production volume or rate are smaller in continuous processes,

* Corresponding author at: School of Chemical, Materials and Biological Engineering, University of Sheffield, Western Bank, Sheffield S10 2TN, UK.
E-mail address: z.kis@sheffield.ac.uk (Z. Kis).

https://doi.org/10.1016/j.ejps.2025.107183
Received 6 March 2025; Received in revised form 7 June 2025; Accepted 24 June 2025
Available online 25 June 2025

Nomenclature

CGE	capillary gel electrophoresis
CPPs	critical process parameters
CQAs	critical quality attributes
DS	drug substance
DP	drug product
EE	encapsulation efficiency, (%)
EL	exposure limit
ELS	electrophoretic light scattering
FRR	flow rate ratio
GC	gas chromatography
HF	hollow fiber
LNPs	lipid nanoparticles
mPES	modified polyethersulfone
NFS	nano flow sizer
RT	room temperature (°C)
RC	regenerated cellulose
SR-DLS	spatially resolved dynamic light scattering
SP-TFF	single pass tangential flow filtration
TEM	transmission electron microscopy
TFR	total flow rate (mL/min)
TMP	transmembrane pressure (psi)
TFF	tangential flow filtration
PDA	particle size distribution (nm)
PDI	polydispersity index

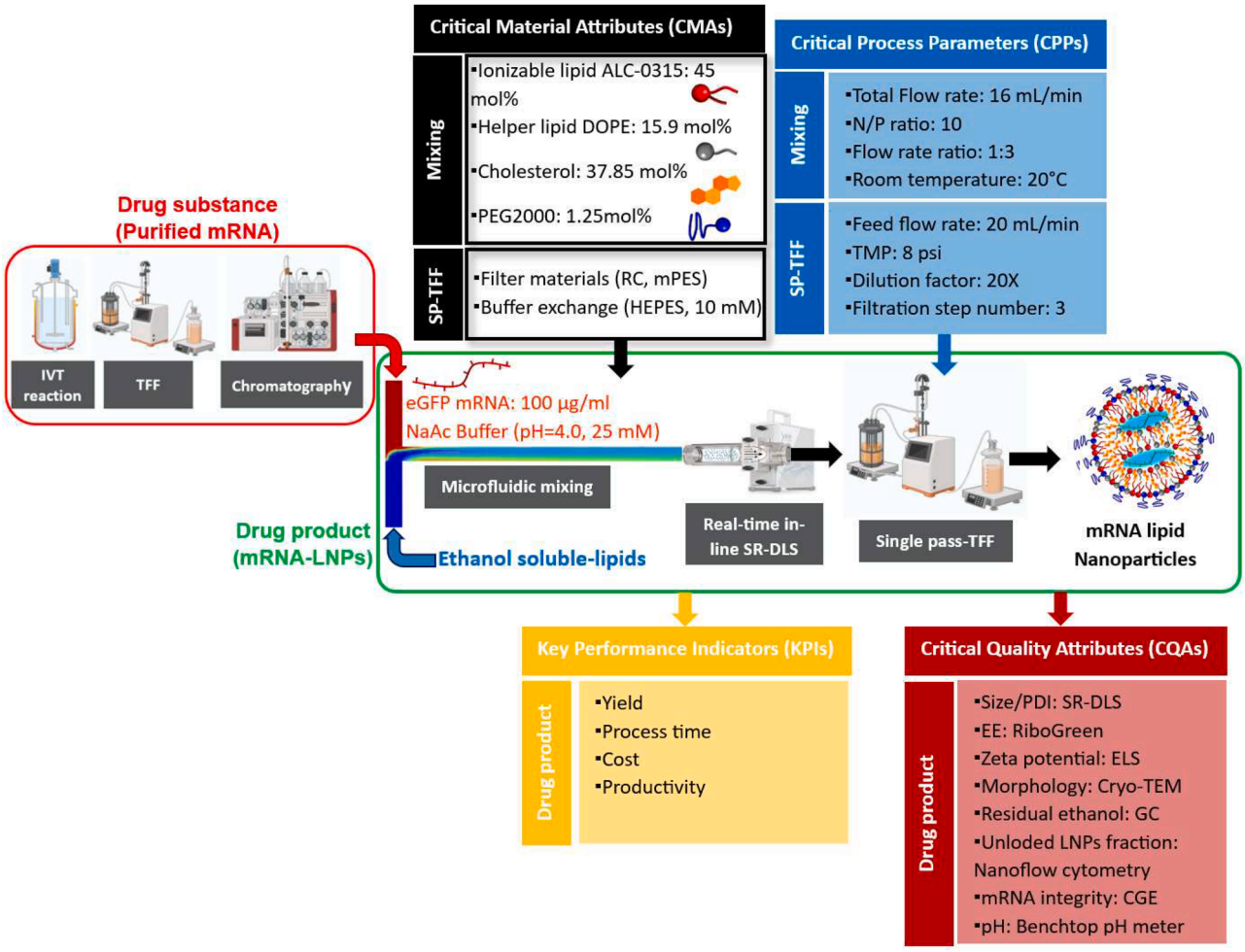

Fig. 1. Continuous mRNA vaccines and therapeutics manufacturing platform process. Formulation reagents, CPPs, CQAs and KPIs are also shown for the mRNA drug product produced in this study by microfluidic mixing, monitored using SR-DLS, and purified by SP-TFF.

contributing to cost reductions. Fourth, continuous manufacturing typically incorporates real-time in-line or on-line analytical technologies, reducing the need for manual sampling and time-consuming off-line analysis common in batch processes. Traditional batch downstream processing for mRNA-LNP production involves separate unit operations, including mRNA-LNPs encapsulation, purification, and sterilization with hold times and testing between these unit operations. In contrast, continuous processing integrates these steps into a single, uninterrupted operation, eliminating intermediate stages and enhancing both efficiency and product quality. Moreover, continuous processes are particularly well-suited to Quality by Design (QbD) principles, which support real-time monitoring and control via the development of mechanistic and deterministic models that mimic process behaviour (Antonio Costa, 2024; Hengelbrock et al., 2023). The integration of QbD with continuous manufacturing can further increase production efficiency, reduce the manufacturing footprint, reduces costs, ensures consistent quality,

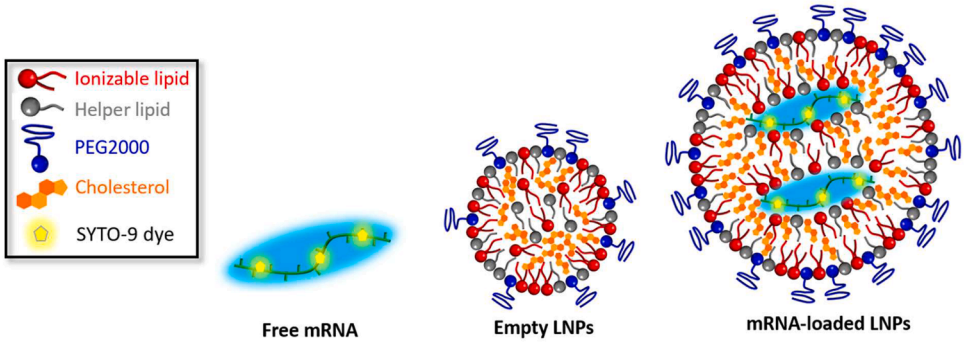

Fig. 2. Intercalation of the SYTO-9 dye into both free and encapsulated mRNA molecules to differentiate between loaded mRNA-LNPs and empty particles.

and supports the delivery of GMP-grade final products. In recent years, continuous mRNA manufacturing processes have started being developed (Nelson, 2023; Arnum, 2024). However, there are still knowledge gaps in optimising and implementing these innovative manufacturing approaches (Eckford, 2023).

The leading method for preparing mRNA drug products (mRNA-DP) involves encapsulating purified mRNA within lipid nanoparticles (LNPs), followed by purification of mRNA loaded-LNPs (Fig. 1). Microfluidic mixing is a widely used technique for manufacturing mRNA-LNPs, whereby lipids dissolved in an organic phase (e.g. ethanol) are combined with the mRNA payload contained in an aqueous buffer (Kimura et al., 2018; Kotouček et al., 2020). The influence of critical process parameters (CPPs) of microfluidic mixing on Critical Quality Attributes (CQAs) of mRNA-LNPs has been the topic of several scientific papers (Ly et al., 2022; Kauffman et al., 2015). Here, the mixing of ethanol and aqueous phases was performed using a high-pressure PEEK T-junction mixer, previously used for the same purpose (Ly et al., 2022). A key novelty of this study is the implementation of a continuous LNP formulation unit operation using the above single-use mixer part, with real-time in-line size and polydispersity index (PDI) monitoring using spatially resolved dynamic light scattering (SR-DLS).

As shown in Fig. 1, the mRNA-LNP product exiting the mixing reaction requires purification. Downstream purification in continuous mode presents greater challenges compared to batch processes, primarily due to potential disturbances that can lead to abnormal process behaviours such as overpressure or overflow (Gerstweiler et al., 2021; Domokos et al., 2021). One specific source of these disturbances is membrane fouling during continuous tangential flow filtration (TFF), which must be carefully assessed and minimized (Malladi et al., 2023). To address this issue, membrane fouling in the continuous purification process was evaluated by using different single-pass TFF (SP-TFF) cassettes. All the mixer and cassette parts are compatible with single-use flow-through processing that can be implemented for GMP-compliant production of mRNA vaccines and therapeutics.

In this article, we aim to advance the mRNA vaccine and therapeutics production process towards a faster, cleaner, and more cost-effective continuous manufacturing platform. We propose technical advances based on industry-embraced products. These findings offer valuable insights for enabling the development of filtration strategies that minimise membrane fouling caused by LNPs while maintaining the CQAs within the desired specifications.

2. Materials and methods

2.1. mRNA-drug product formulation

A modified eGFP mRNA formulation based on the Pfizer/BioNTech COVID-19 vaccine formulation was used for mRNA encapsulation (Fig. 1) (Schoenmaker et al., 2021; Highlights of Prescribing Information, 2021). The ethanol and mRNA aqueous phases were combined in a T-junction mixer at the optimum process conditions we explained in our previous study (Ly et al., 2022). The formulation batch mixing was done using a Chemyx Fusion 4000 syringe pump while continuous mixing was done by a Vapourtec R-Series modular flow chemistry system at room temperature (RT: 20.0 ± 0.5 °C, Fig. S1A supplementary document). The eGFP mRNA was purified by Akta PCC chromatography and concentration was measured by HPLC spectrophotometer before the mixing process as described in our other studies (Qu et al., 2024; Welbourne et al., 2024). To adjust the buffer pH to neutral, 25 w/w% PBS buffer (1 M) was added to the mRNA-LNPs product immediately after the mixing reaction. Due to the high cost of mRNA-LNPs, some tests involving flow size measuring were performed with nanoliposomes. The nanoliposomes were synthesized using the same approach but with just two changes in the formulation recipe: (1) the high-cost ionisable lipid was substituted with the helper lipid, and (2) no mRNA was in the aqueous buffer.

2.2. mRNA drug product purification

After the mixing reaction, the mRNA-LNPs product contains 25 % ethanol concentration, which was separated using a benchtop TFF system (KrosFlo® KR2i, Repligen, Fig. S1B supplementary document). The modified polyethersulfone hollow fiber (mPES-HF) filter (Repligen, Product number: C02-E300–05-N 300 kDa, 20 cm^2) was used for performing the batch TFF process. The polyethersulfone cassette filter (Sartocon, 300 kD /50 cm^2) and cellulose-based cassette filter (Hydrosart 300 kD /50 cm^2), both from Sartorius, were used for continuous purification at RT. The measured zeta potential of mRNA-LNPs was in the range of −15– −20 mV. Both SP-TFF cassette types are hydrophilic and have negative surface charges, which makes them suitable candidates for the separation of LNPs with the negative surface charge (Abd-Razak et al., 2021).

2.3. mRNA drug product characterisation

NanoFlowSizer (NFS). NFS was used for the real-time in-line size characterization of mRNA-LNPs. NFS uses a spatially resolved dynamic light scattering (SR-DLS) technique that enables the measurement of particle size during continuous flow (Besseling et al., 2019). A standard suspension of monodisperse polystyrene nanoparticles (100 nm mean diameter and SD: 5 nm, Sigma-Aldrich) was used for the calibration of the NFS before each size analysis. The viscosity of the ethanol-water mixture for size analysis was extracted from data in the literature (Furukawa and Judai, 2017).

Encapsulation efficiency (EE). RiboGreen® assay (Invitrogen, Catalog Number: R11490) was used according to the manufacturer's instructions as a standard method for the quantitation of EE of eGFP mRNA in LNPs. A Tecan plate reader (Infinite® 200 PRO) was used to read the fluorescence of the RiboGreen dye at Excitation/Emission of 485/530 nm. The high-range assay that allows quantitation of 20 ng/mL to 1 μg/mL eGFP mRNA was used for RiboGreen test and the EE was

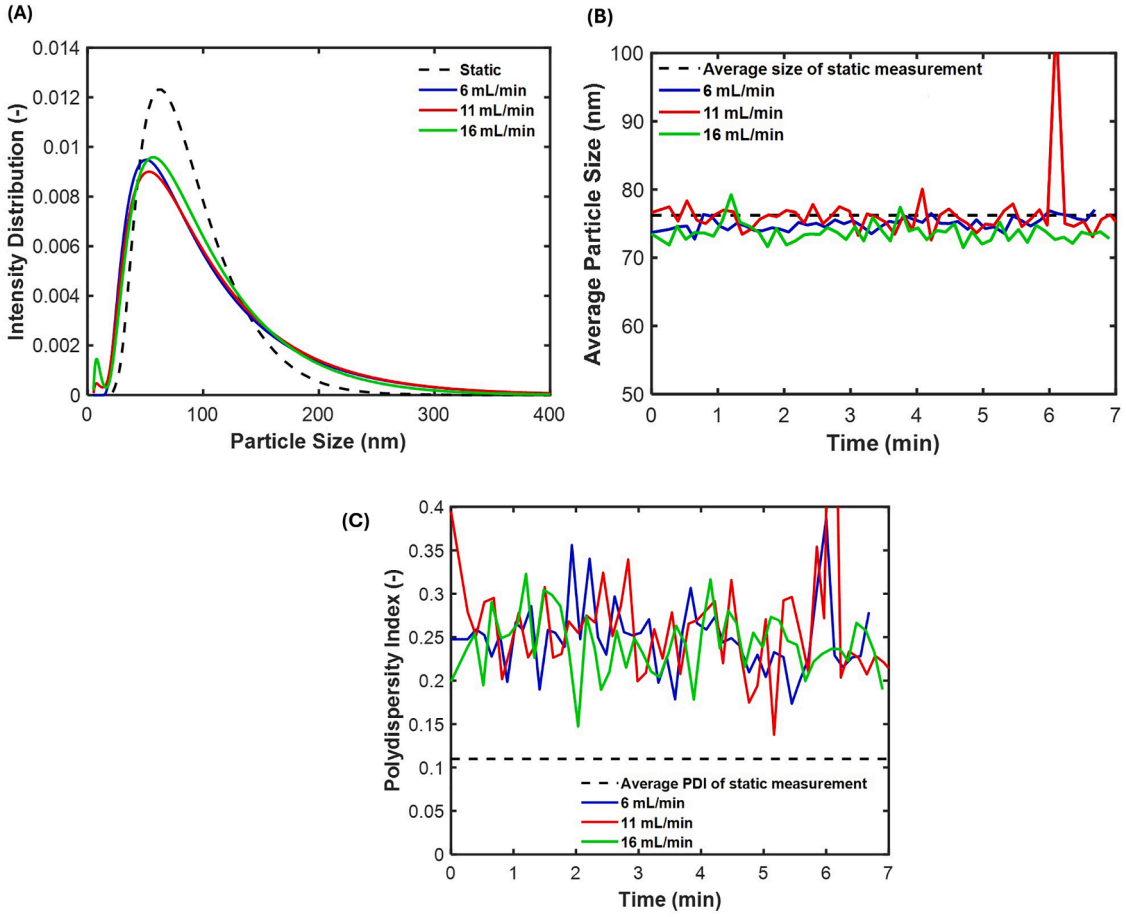

Fig. 3. Particle size distribution (PSD) and polydispersity index (PDI) measurement of LNPs using spatially resolved dynamic light scattering (SR-DLS): (A) PSD measurement in both static and flow modes, (B) average PSD and (C) PDI of LNPs over time. The tests were conducted by circulating pre-fabricated nanoliposomes (average size: 76 nm) at varying flow rates.

calculated as follows (Jones et al., 1998):

$$EE(\%) = \frac{mRNA_{total} - mRNA_{free}}{mRNA_{total}} \times 100 \quad (1)$$

where $mRNA_{total}$ is the concentration measured after solubilizing mRNA-LNPs using Triton X-100 surfactant to release the encapsulated mRNA. $mRNA_{free}$ is the concentration of free mRNA in the solution and the mRNA potentially adsorbed to the LNP's surface.

Nano-flow Cytometry (NanoFCM). NanoFCM is a quantitative, multi-parameter characterisation technique applied to measure multiple CQAs of mRNA-DP. The system calibration was performed with standard samples before each measurement. The standard Quality Control (QC) bead solutions of SiNPs (250 nm) and S16M Exo (68–155 nm) were used for concentration and size calibration, respectively.

The NanoFCM benefits from a two lasers analyser (Blue 488 nm and Red 640 nm) that enables it to simultaneously measure LNP's physical properties (e.g. size and concentration/number) and differentiate mRNA-loaded LNPs from empty ones when particles are exposed to laser excitation. A SYTO-9 dye (Excitation/Emission: 483/503 nm, Invitrogen: S34854) was employed for this purpose. SYTO-9 can intercalate to both free and encapsulated mRNA molecules via penetrating LNPs structure as schematically illustrated in Fig. 2. The dye generates stronger fluorescence intensity when bonded to the mRNA molecules than when free in the buffer solution. For an optimal measurement, fresh 10 mM HEPES was used as the diluent buffer (9 μL HEPES + 1 μL SYTO 9 at 10x optimal concentration). Further information about preparation of mRNA-LNPs for analysis using NanoFCM was provided in the supplementary document. The procedure was used for the preparation of both empty and mRNA-loaded nanoparticles.

Cryogenic Transmission Electron Microscopy (Cryo-TEM). At first, the mRNA-LNPs were diluted to a total lipid mass concentration of ~10 mg/mL. Cryo grids were prepared using a Leica EM GP automatic plunge freezer (Leica Microsystems). Diluted mRNA-LNP sample (5 μL) was deposited onto copper grids coated by a lacey carbon film. Excess liquid was blotted for 5 s from the grid side and then vitrified by plunging into liquid ethane. Frozen grids were kept in liquid nitrogen until imaged using Tecnai Arctica TEM operated at 200 kV.

Gas Chromatography (GC). Residual ethanol concentration after the TFF purification was measured using Gas Chromatography with a Flame Ionization Detector (FID) (TRACE 1300, Thermo Scientific) equipped with a TRACE™ TR-FFAP GC Column (TPA-modified polyethylene glycol). Ethanol (Sigma-Aldrich) and water standards were used for generating a calibration curve in volume percentage (v/v). GC conditions were as follows: flow rate 1 mL/min, 0.1 μL injection, isothermal at 110 °C, and inlet temperature at 220 °C (Weatherly et al., 2014).

LNPs Zeta potential and pH *measurement.* The zeta potential and pH of LNPs were measured using Stabino Zeta (Microtrac, Germany) and Benchtop Orion Star A111 (Thermo Scientific), respectively.

mRNA integrity. The encapsulated mRNA was released from LNPs by mixing particles with an equal amount of Triton 100X surfactant (1 v/v % in TAE buffer 1X) followed by incubation for 30 min at RT. The eGFP mRNA was then separated from other ingredients using Monarch® RNA Purification Columns. The integrity of purified eGFP mRNA was analysed using capillary gel electrophoresis (CGE) on an Agilent 5200 Fragment Analyzer instrument with the Agilent RNA Kit (15 nt) (Welbourne et al., 2024a). The errors of the CGE methods are provided

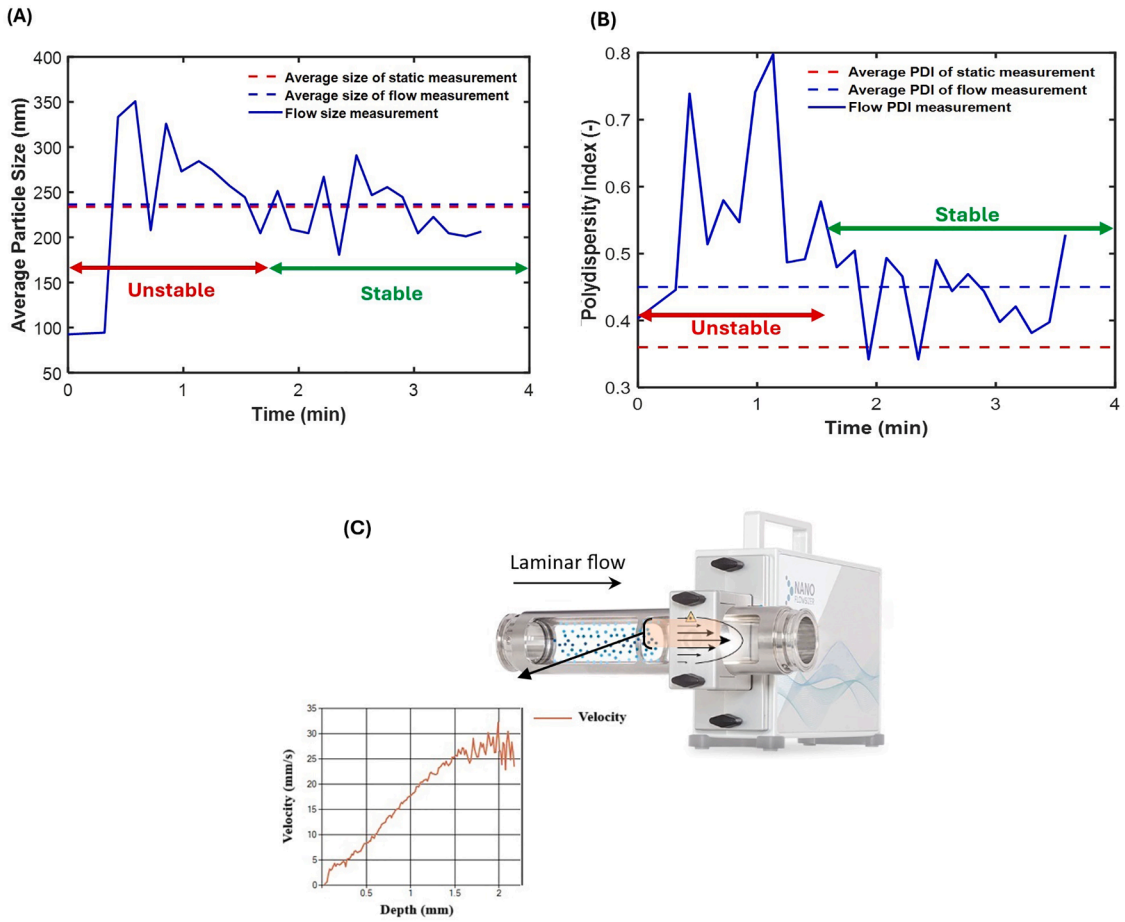

Fig. 4. Real-time in-line monitoring of LNP quality attributes in a continuous mRNA-LNP production process: (A) average particle size distribution (PSD) and (B) Polydispersity Index (PDI) of mRNA drug product measured at static and flow (16 mL/min) modes using the Nano Flow Sizer (NFS) instrument. (C) Velocity profile across the NFS tube radius when the reaction mixture filled the tube and the laminar flow fully developed.

in Table S1.

3. Results and discussion

3.1. Batch and continuous flow LNP formation monitored by static and in-line flow size measurement

The microfluidic mixing experiments were performed in both batch and continuous modes. For static measurement, a sample vial holder was used for the off-line size measurement while, as can be seen in Fig. S1A, a flow cell module was used for in-line size measurement during the continuous process. The size and PDI measurement of mRNA-LNPs should ideally be checked pre- and post-TFF. However, given the high cost of SR-DLS, it is not practical to install two inline instruments, one upstream and another downstream of the TFF unit. To address this, inline size measurement is performed immediately after microfluidic mixing and prior to the TFF step, ensuring that LNP formation occurs as intended. Post-TFF size and PDI measurement is then conducted offline in static mode for process characterisation to confirm that particle integrity is maintained throughout the purification process. For the employed flow cell (0.5 in. ID), the bulk Reynolds number of $Re \sim 30$ was calculated for the flow rate 16 mL/min, confirming laminar flow across the cell during in-line size measurement. As part of initial tests, a set of flow size measurements were performed by the circulation of pre-fabricated nanoliposomes (average size 76 nm) at different flow rates (6, 11, and 16 mL/min). Fig. 3A shows the Particle Size Distribution (PSD) of the nanoliposomes measured by NFS for static and flow measurements. Fig. 3B and C show the average size and Polydispersity Index (PDI) over time, respectively. The most important observation was that the measured PDI in flow mode was higher than the static measurement (off-line analysis). As a matter of fact, the NFS flow mode samples sparse populations of (large) particles in a more effective way. This is because the exposure of larger particle populations to the DLS laser statistically increases in flow measurement. For this reason, it suggests comparing static-to-static and flow-to-flow measurements for absolute comparisons. This point should be considered when the new regulator or regulatory framework is being set up for a continuous mRNA-DP manufacturing platform unless the accuracy of the flow PDI measurements is improved.

The continuous manufacturing of mRNA-LNPs was performed using the procedure explained in section "2–1-Drug product formulation".

Figs. 4A and B show the average PSD and PDI of mRNA-DP overtime during the mixing reaction at optimum flow rate 16 mL/min, respectively. At the start of the mixing reaction, the measurement conditions were initially unstable due to the time required to fill the NFS flow cell (indicated by the red arrow in Fig. 4A and B). Based on the geometry of the flow cell, 1.27 cm in diameter and 8 cm in length, and a flow rate of 16 mL/min, approximately 40 s were needed to fully fill the cell. Once filled, laminar flow was established, allowing the SR-DLS measurements to stabilize and increase in precision. Fig. 4C shows the velocity profile across the NFS tube radios when the tube was filled with the reaction mixture and the laminar flow fully developed. A linear velocity profile confirmed an ideal condition for the size measurement. Due to materials availability constraints, the continuous mixing reaction was performed for just a few minutes. One of the main challenges in continuous mixing operation was the occasional pressure buildup, indicating a blockage in

Table 1
Experimental TFF tests for mRNA-LNP buffer exchange in both batch and continuous format.

Test mode	TMP set-point (psi)	Filter type	Flow rate	Procedure
Batch	8	mPES hollow fiber (300 kDa)	20 ml/min	10X con. followed by 5X diafiltration and 2 washing steps
Continuous	8	Polyethersulfone cassette filter (Sartocon, 300 kD /50 cm^2)	20 ml/min	Three consecutive SP-TFF diafiltration and a final washing step
Continuous	8	Cellulose based cassette filter (Hydrosart, 300 kD /50 cm^2)	20 ml/min	Three consecutive SP-TFF diafiltration and a final washing step

the T-junction mixer. This obstruction disrupted the smooth flow and, in some cases, completely halted mixing. The observed pressure increase and flow blockage could be attributed to the formation of larger particles in the flow path. To solve this problem, a bigger capillary pipe diameter was used for lipid injection through a T-mixer in continuous manufacturing tests. A better design of the mixer or applying a more efficient mixing technique (e.g. impingement jet mixing) could possibly be beneficial for carrying out a robust continuous mRNA-DP production process.

3.2. Purification of mRNA-LNPs using TFF

It has been reported that ethanol could have an adverse impact on LNP stability by penetrating into the particle structure and dissolving non-polar lipids over time (GY, 1985; Hardianto et al., 2023). Kimura et al. demonstrated that reducing the residual ethanol in the LNPs prevents the undesirable aggregation or fusion of LNPs (Kimura et al., 2020). Moreover, the level of class 3 residual solvents (i.e. less toxic, such as ethanol) should be kept below a certain exposure limit (EL) of 5000 ppm in the final mRNA-DP (I.H.T.J.C.S. Guideline 2005). Therefore, buffer exchange and residual ethanol removal from mRNA-LNPs is a crucial downstream purification operation that can be carried out by filtration or dialysis. TFF purifications are typically accomplished at constant transmembrane pressure (TMP) (Bowen and Gan, 1991; Buetehorn et al., 2010). Table 1 shows the experimental conditions of the TFF tests carried out at constant TMP in batch and continuous modes. Traditional TFF operates in batch mode by recirculating the feed (mRNA-LNPs) through filters, offering greater flexibility in process design compared to continuous TFF. This is because batch processes are not constrained by the need to manage upstream flow entering the TFF unit. In the continuous SP-TFF, the recirculation loop of the batch process is eliminated, while feed residence time in the membrane is increased, allowing a wide range of concentration factors to be achieved (Marino et al., 2017; Dizon-Maspat et al., 2012).

An Automatic Backpressure Valve (ABV) on the retentate line was used to adjust and control the TMP at the set point. The feed was prepared by dilution of mRNA-LNPs with HEPES buffer (10 mM, pH 7). A multi-consecutive SP-TFF filtration approach was applied to estimate

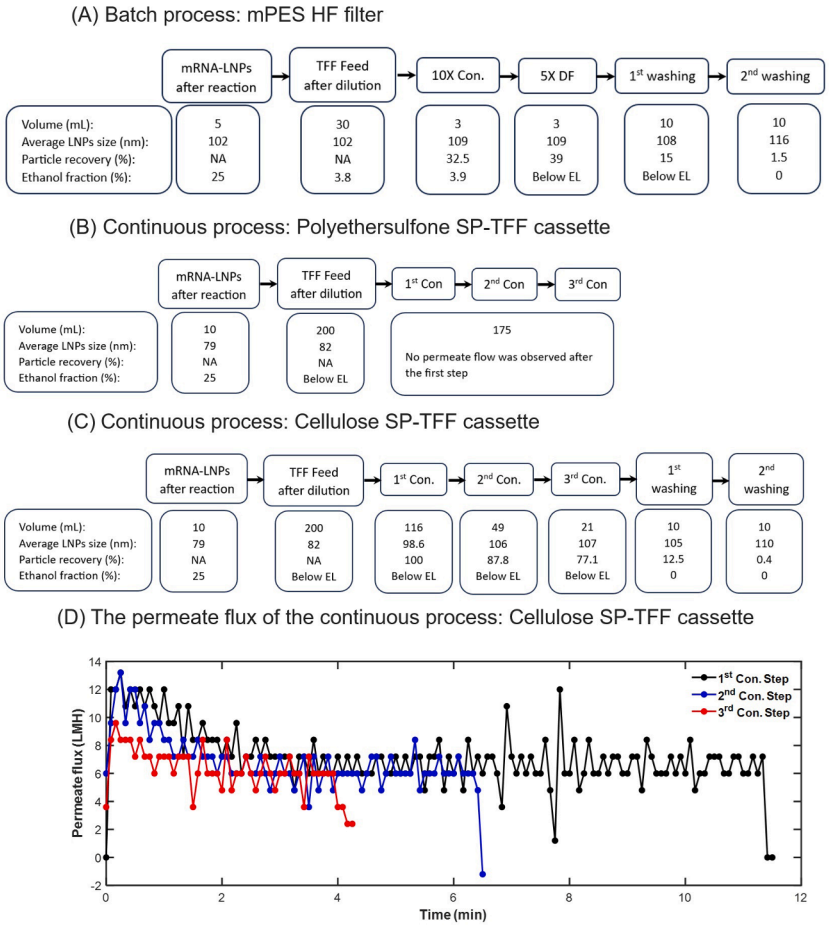

Fig. 5. Quantitative analysis of the retentate during multistep filtration of mRNA-LNPs in (A) batch mode using mPES HF filter (B) continuous process by polyethersulfone SP-TFF cassette and (C) continuous process by cellulose SP-TFF cassette. (D) The permeate flux through the regenerated cellulose (RC) cassette over time at different concentration steps.

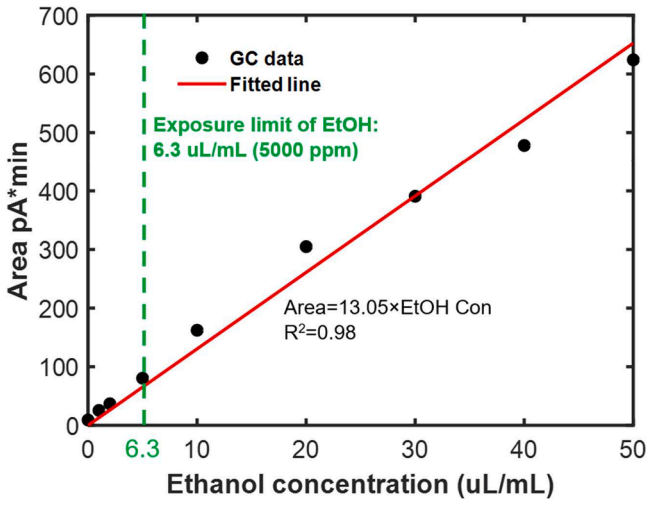

Fig. 6. The experimental linear range of peak area response vs. ethanol concentration. Ethanol showed a linear response that yielded linear fit equation Area = 13.05 × EtOH with an R-square of 0.98.

the required number of cassette filters (i.e., the total surface area of the filter) to achieve the desired concentration factor. In this way, the collected retentate of a continuous SP-TFF step was used as feed for the next SP-TFF filtration step (Fig. 5B and C).

The permeate collected from the filtration of the mRNA-LNPs was analysed using NFS and Ribogreen tests. No lipid particles and mRNA were detected in the collected permeate, showing complete separation of the DP using 300 kDa cut-off membranes. A typical three consecutive TFF steps including concentration, diafiltration (DF), and washing were applied for the separation of ethanol from DP in batch mode. For analysis of ethanol content, a GC calibration curve (Fig. 6) was generated using a set of standard sample mixtures of pure ethanol and water. The calibration curve was then used for the measurement of residual ethanol at different steps of the TFF process. The green line in Fig. 6 shows the exposure limit of ethanol concentration in the final mRNA-DP, also known as residual ethanol CQA (Kimura et al., 2020; I.H.T.J.C.S. Guideline 2023).

In batch mode, a 6X dilution of post-mixing mRNA-LNPs using HEPES buffer (10 mM, pH 7) followed by 10X concentration and 5X DF reduced ethanol concentration from 25 % to below the exposure limit.

For the continuous TFF process, 20X dilution of original mRNA-LNPs using HEPES buffer (10 mM, pH 7) was undertaken to reduce ethanol from 25 % to below the exposure limit. Then, three consecutive continuous single-pass concentration steps were performed to concentrate the mRNA-LNPs. The result of the TFF tests is shown in Fig. 5. The efficiency of continuous separation using PES SP-TFF cassette was unsatisfactory since no permeate flow was observed after the first concentration step (Fig. 5B). In fact, a phenomenon prevents the feed flow from passing through the cassette pores, and the main culprit for such observation is the fouling of the membrane surface by LNPs during the first concentration step. In contrast to PES, with the RCSP-TFF cassette, 90 % of mRNA-LNPs were recovered after three consecutive concentration steps (Fig. 5C), achieving a 10X overall concentration factor. The total recovery was determined by summing the amount of mRNA-LNPs collected in the final filtration step with the amount recovered from the tubes and filter during the initial washing step. The percent of recovery was calculated using the total number of mRNA-LNPs before and after the TFF process which were measured using NanoFCM. The total recovery of mRNA-LNPs for batch process using HF filters was 54 % (Fig. 5A). The lower recovery observed in batch TFF (54 %) compared to continuous SP-TFF (90 %) may be attributed to membrane fouling and particle retention within the recirculation loop. Further optimisation of batch filtration conditions could mitigate these losses. The permeate flux through the RC cassette over time at different concentration steps is shown in Fig. 5D As a rule of thumb, if the SP-TFF cassette fouls, the

Table 2
CQAs of mRNA-LNPs measured before and after the TFF process in batch and continuous modes.

	Batch process		Continuous process	
	Before TFF	After TFF	Before TFF	After TFF
Average size by NFS (nm)	64	107	89	105
PDI by NFS (-)	0.16	0.15	0.14	0.10
Average size by NanoFCM (nm)	72	118	99	124
Total mRNA-LNPs recovery (%)	-	54	-	90
EE (%)	88.8	95.6	89.6	95.5
Loaded mRNA-LNPs fraction (%)	98.2	99.8	99.9	99.6

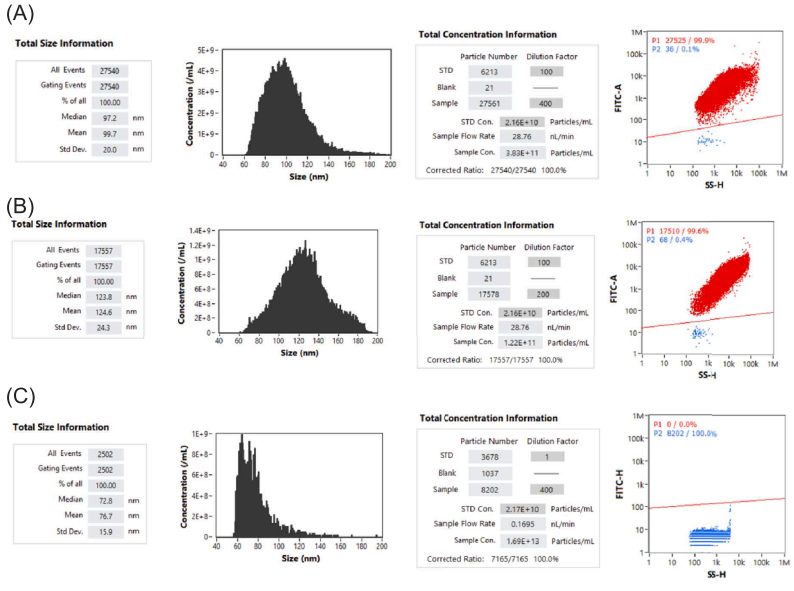

Fig. 7. The size analysis of mRNA-LNPs using NanoFCM (A) before TFF, (B) after TFF, and (C) comparative size analysis of empty liposomes before TFF.

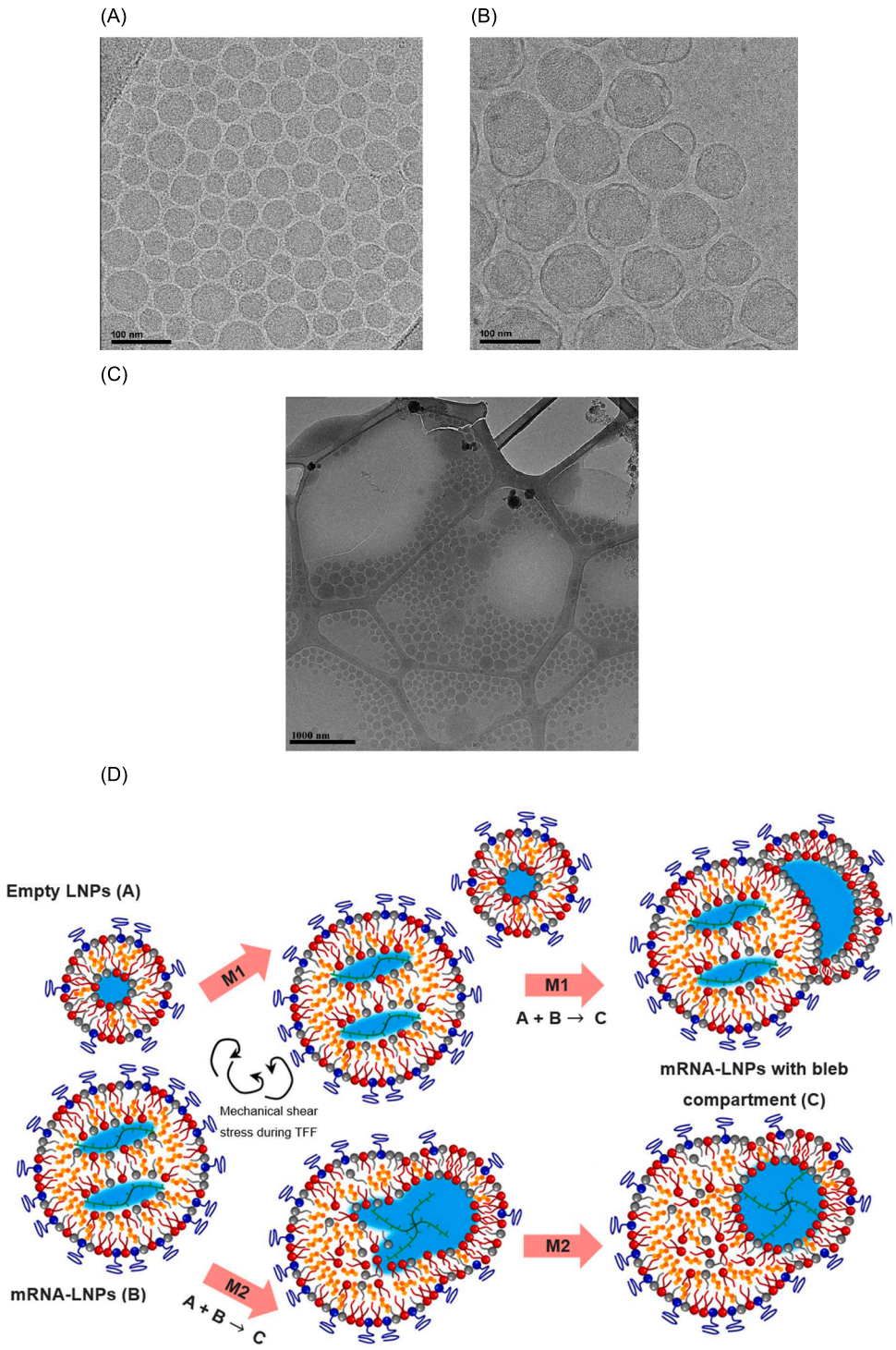

Fig. 8. Cryo-TEM of mRNA-LNPs (A) before and (B and C) after the TFF process. The TFF process was performed to remove ethanol using 300 kDa mPES HF filter. (D). Illustration of the most probable mechanisms (M1 and M2) of bleb compartment formation on the surface of LNPs during the TFF process (the proposed mechanisms were adapted from (Cheng et al., 2023a; Simonsen, 2024)).

permeate flux will decline (Miller et al., 2014; Aimar et al., 1989). However, here, in Fig. 5D, no change in permeate flux was observed over time for different concentration steps after stabilizing the TMP set point, which implies that no significant membrane fouling occurred. The result provides useful information for researchers for selecting the membrane type and designing a continuous approach (e.g., step numbers, feed flow rate and TMP) to achieve the desired concentration factor.

3.3. mRNA-LNPs characterization before and after the TFF

Nano-FCM in combination with SYTO-9 dye for mRNA labelling was used to determine the portion of loaded mRNA-LNP post-mixing (Fig. 7A) using nanoliposome as an empty control (Fig. 7C). Determination of the unloaded mRNA-LNP fraction is important because empty particles can induce an inflammatory response inside the body (Moghimi and Simberg, 2022). Fig. 7A confirms that a tiny fraction of LNPs (<1 %) is empty (i.e. does not contain mRNA) post-mixing. Size

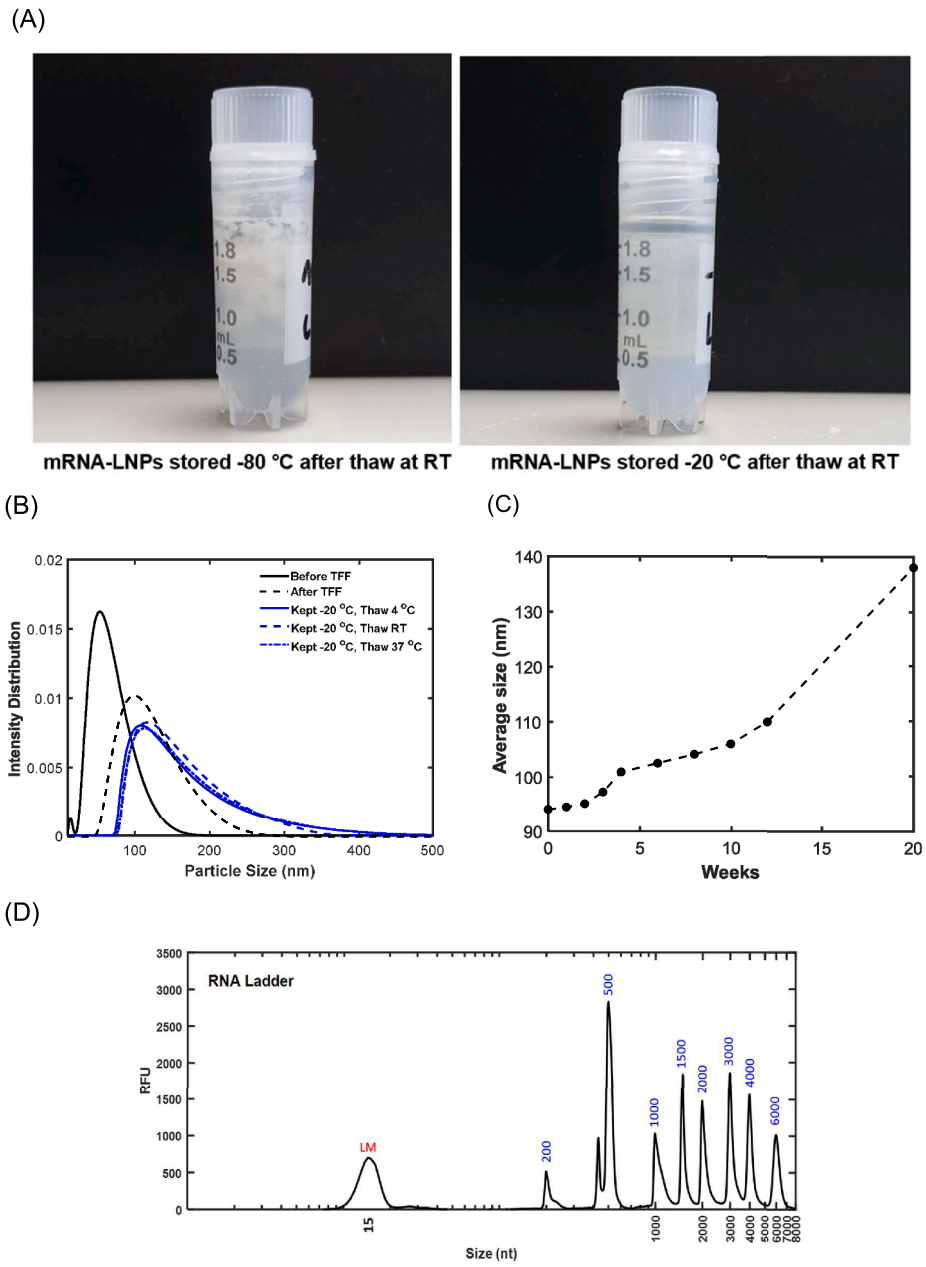

Fig. 9. Effect of storage temperature on mRNA-LNPs stability. (A) mRNA-LNPs sample stability after 15-day storage at -80 and -20 °C, (B) particle size distribution of mRNA-LNPs stored at -20 °C after thawing at 4, RT ad 37 °C, (C) mRNA-LNPs average size stored at 4 °C as a function of time. (D) The electropherograms of the purified eGFP mRNA (released from LNPs) immediately after mixing reaction, TFF process and, after storing at 4 °C for 30 days. X-axis in electropherograms shows the nucleotides size (nt) and Y-axes (relative fluorescence units, RFU) show the mRNA amount at a certain size/time. The eGFP mRNA peak (~1000 nt; blue), and the lower marker (LM ~15 nt; red) are indicated.

and loading of mRNA-LNPs were also compared pre (Fig. 7A) and post-TFF (Fig. 7B) process. TFF did not affect the percentage of mRNA-loaded particles versus empty particles. However, an increase in mRNA-LNP size was noted. The increase in size was confirmed by orthogonal methods, using NFS, NanoFCM (Table 2) and cryoTEM (Fig. 8). The size increase of LNPs seems to be due to the merging of small particles into large ones, and in some cases, the formation of blebs compartment on the particle surface (discussed later in this section). In fact, a considerable shear is applied onto small particles during the TFF process inside filters that forces them to agglomerate or be adsorbed by relatively bigger particles.

The mRNA encapsulation efficiency (encapsulated versus free mRNA) was analysed by Ribogreen assay (Table 2) and shows a high efficiency of encapsulation post-mixing for both the batch and the continuous formulation process. The increase in EE after the TFF process (Table 2) was observed for both batch and continuous modes of TFF operation. The increasing EE could be due to two different reasons. The first probable reason is membrane fouling with free eGFP mRNA which reduces the total number of unencapsulated mRNA molecules in the Ribogreen analysis. The less likely reason is the merging of free eGFP mRNA molecules into the bleb compartments because of applied shear stress during the TFF process, which increases EE.

Cryo-TEM was used to investigate the structural features of the mRNA-LNPs before and after TFF filtration that is shown in Fig. 8 (the TEM images with a larger size were provided in Fig. S2 in the supplementary document). The size ranges of LNPs before and after the TFF

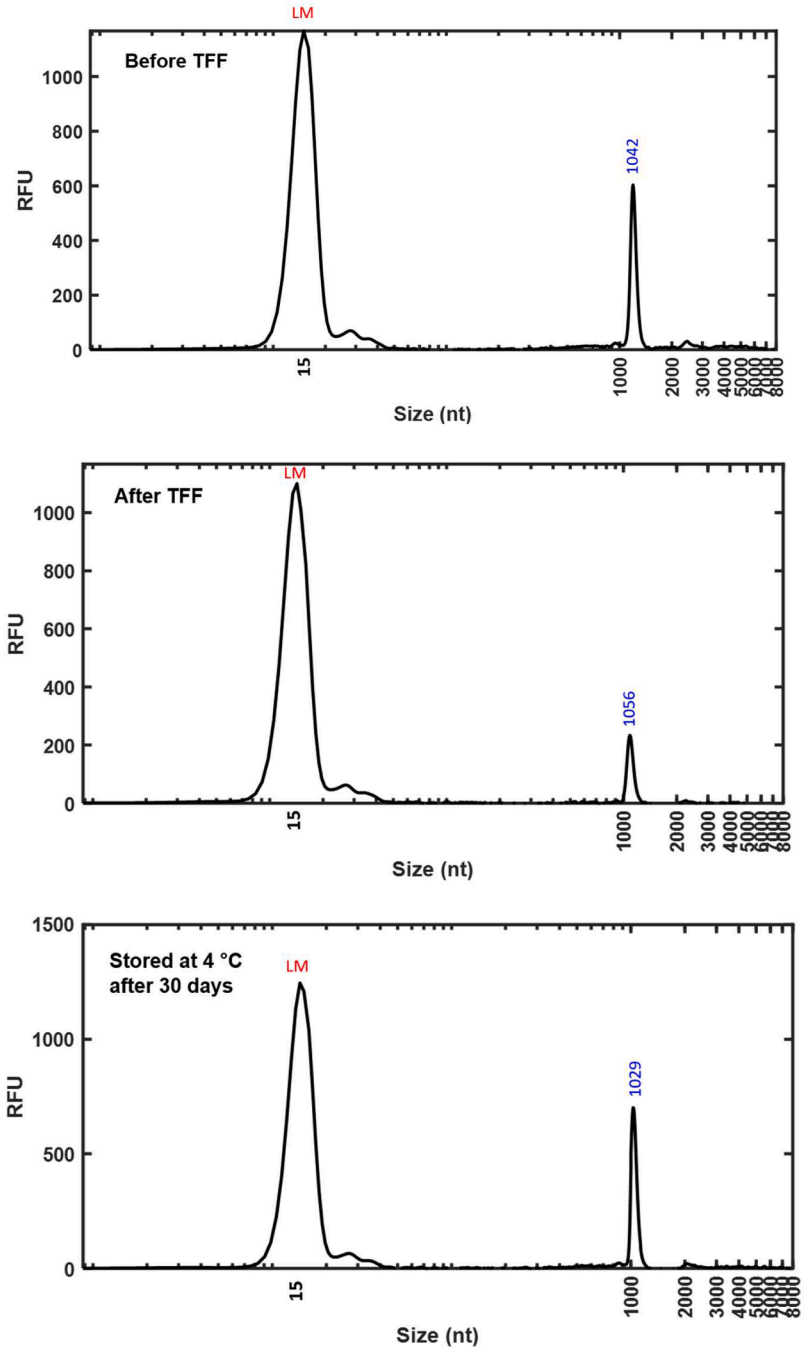

Fig. 9. (*continued*).

process measured using cryo-TEM matches the size ranges measured by dynamic light scattering (DLS) using the NFS and by nano flow cytometry using the NanoFCM (Table 2). The presence of vesicular structures can vividly be observed in TEM images (Reinhart et al., 2023).

The Cryo-TEM images (Fig. 8B and C) also show the mRNA-LNPs structure after TFF purification involving solvent pockets associated with the formation of bilayer lipids on the particles surface, which are called blebs (Leung et al., 2015). The most likely mechanisms of bleb compartment formation on the surface of LNPs are illustrated in Fig. 8D. Brader et al. (2021) applied the Cryo-TEM analysis of dye-stained mRNA-LNPs to show that the mRNA can transfer to the bleb compartment by dissociation from the ionisable lipid inside the LNPs structure. Cheng et al. (2023b) reported that mRNA-rich bleb structures improve the mRNA transfection efficiency in both *in vitro* and *in vivo*. One of the proposed reasons for the improvement of mRNA transfection potency is attributed to the fact that the bleb compartment acts as a shield and protects the mRNA molecule structure against degradation due to oxidation or alkylation when it is in direct contact with lipid molecules (Yan and Zaher, 2019). The evaluation of the transfection potency of the manufactured mRNA-LNPs is under investigation and will be published in a separate study.

3.4. *mRNA-LNPs stability analysis over time*

mRNA DP formulations are sensitive to environmental factors. In particular, mRNA is very fragile. At neutral or slightly alkaline pH-conditions typical of current mRNA vaccine formulations-mRNA degradation primarily occurs through the cleavage of phosphodiester

bonds in the RNA backbone. This process is driven by a transesterification reaction, where the adjacent 2′-hydroxyl group of the ribose moiety facilitates bond breakage by attacking the phosphorus center of the 3′,5′-phosphodiester linkage (Mikkola et al., 2018; Lehmann and Schmidt, 2003). This reaction is facilitated at elevated temperatures (Li and Breaker, 1999). Moreover, temperature fluctuations and inadequate storage can cause lipid oxidation or aggregation of the LNPs which may reduce their effectiveness *in vivo* (Chheda et al., 2024). Kim et al. (2023) reported that mRNA-LNPs stored in 10 % w/v sucrose as cryoprotectant in PBS at -20 °C remained stable for at least 30 days. In contrast, LNPs stored at -80 or -200 °C (flash frozen in liquid nitrogen) showed significant aggregation after melting (Kim et al., 2023). In another recent study Kafetzis et al. (2023) examined the impact of storage conditions on mRNA-LNPs formulated vaccines, focusing on maintaining structural integrity and functionality. The results show that the size of mRNA-LNPs stored at −80 °C without cryoprotectant agent significantly increased after two weeks (Kafetzis et al., 2023).

Here, the purified samples after the TFF process were stored at different temperatures of 4, -20 and -80 °C. The samples stored at -20 and -80 °C were then thawed at temperatures of 4 °C, 20 °C (RT) and 37 °C. The samples were frozen once, kept frozen for 30 days and then thawed once. All LNP samples stored at -80 °C completely destabilized and creaming phenomena occurred at all investigated melting temperatures (Fig. 9A). Incorporating sucrose or other stabilizers may mitigate this effect and should be investigated in future work. On the other hand, samples stored at -20 °C were stable even without adding any cryoprotectant agent. Furthermore, no significant effect of thawing temperature on LNPs size was observed on samples stored at -20 °C as shown in Fig. 9B The RiboGreen assay data indicate that the encapsulation efficiency (EE) and mRNA concentration were 95.5 ± 3.3 % and 83 ± 5.5 ng/μL, respectively, prior to freezing. After 30 days of storage at -20 °C and subsequent thawing, the EE was 88.9 ± 3.8 % and the concentration was 70.7 ± 4.9 ng/μL, respectively. Fig. 9C illustrates the average size of the sample stored at 4 °C as a function of time. The data shows 3, 9, and 17 % of increasing average size in the first three storage months and 47 % after 5 months of keeping the sample at 4 °C. The CGE electropherograms provided in Fig. 9D confirm no change in eGFP mRNA integrity during the TFF process and up to 30 days after the storage at 4 °C. Based on technical replicates of CGE analysis, the mRNA integrity was 97 ± 2.1 % before storage and 96.5 ± 3.2 % after 30 days of storage at -20 °C followed by thawing.

4. Conclusion

The shortage of vaccine doses during the COVID-19 pandemic underscored the bottlenecks in mRNA vaccine manufacturing, and since then the development of RNA based vaccines and therapeutics has skyrocketed. This highlights the urgent need for the development of more productive and scalable manufacturing processes, for which continuous manufacturing can provide a viable option. This study introduces improvements in continuous LNP formulation, real-time in-line particle size and PDI monitoring, and single-pass mRNA-LNP purification by TFF. The integration of these innovations can reduce holding times between unit operations, thereby intensifying the mRNA-DP manufacturing process. This study introduces and evaluates single-use parts (mixer and SP-TFF filters) as agile and flexible equipment for developing continuous processes, while discussing the relevant challenges. Applying single-use parts improves the flexibility of the process, can reduce the up-front investment cost, and eliminates the need for pre-processing sterilisation and post-processing cleaning and cleaning validation. Notably, this study demonstrates the first application of in-line size characterization of mRNA-LNPs within a continuous manufacturing process. The critical quality attributes (CQAs) of mRNA-LNPs were assessed and compared between batch and continuous TFF modes, providing valuable insights for advancing mRNA production technologies. In the continuous mRNA-LNP formulation process, after SP-TFF, the encapsulation efficiency was 95.5±4 %, the average size was 105±6 nm, the PDI was 0.1±0.02, the residual ethanol content after SP-TFF was 0.003 %, the unloaded LNP fraction was 0.4±0.05 % and the mRNA integrity was 86.2±3 %, and the final pH was 7.0. The losses in the SP-TFF using the RC membrane were 10 %. Bleb compartments were also observed on the TFF-purified mRNA-LNP surface using cryo-TEM. To our knowledge, this is the first publication describing the integration of continuous mRNA-LNP encapsulation, real-time in-line particle size and PDI monitoring using spatially resolved dynamic light scattering and single-pass TFF purification. Therefore, this study will enable the more efficient, rapid and high-volume continuous manufacturing of high-quality mRNA vaccines and therapeutics.

CRediT authorship contribution statement

Ehsan Nourafkan: Methodology, Formal analysis, Conceptualization, Writing – original draft, Investigation, Data curation. **Zidi Yang:** Methodology, Writing – review & editing. **Mabrouka Maamra:** Project administration, Writing – review & editing. **Zoltán Kis:** Supervision, Project administration, Methodology, Conceptualization, Writing – review & editing, Funding acquisition.

Declaration of competing interest

The authors declare no competing financial interests or personal relationships that could have appeared to influence the work reported in this paper.

Acknowledgments

This study was funded by Innovate UK, Project Category: Small Business Research Initiative, Project Reference: 10085632. The funder played no role in study design, data collection, analysis and interpretation of data, or the writing of this manuscript. The work was supported by the School of Chemical, Materials and Biological Engineering (formerly Department of Chemical and Biological Engineering), University of Sheffield, UK. The authors also thank James Grinham, Manoj Pohare, Kate A Loveday, Emma N Welbourne and Amodo Design Ltd. (Sheffield) for helpful discussions and assistance.

Supplementary materials

Supplementary material associated with this article can be found, in the online version, at doi:10.1016/j.ejps.2025.107183.

Data availability

Data will be made available on request.

References

Abd-Razak N.H., Pihlajamäki A., Virtanen T., Chew Y.J., Bird M.R.J.F., Processing B., The influence of membrane charge and porosity upon fouling and cleaning during the ultrafiltration of orange juice, 126 (2021) 184–194.

Aimar P., Howell J., Turner M.J.C.E.R., design, Effects of concentration boundary layer development on the flux limitations in ultrafiltration, 67 (1989) 255–261.

Antonio Costa, M.J., 2024. The New Continuous and Controlled Approach to Nanoparticle Processing. BioProcess International.

Arnum, P.V., 2024. Continuous mRNA Manufacturing: Is It the Next Wave in Manufacturing Innovation? DCAT Value Chain Insights.

Besseling R., Damen M., Wijgergangs J., Hermes M., Wynia G., Gerich A.J.E.J.o.P.S., New unique PAT method and instrument for real-time inline size characterization of concentrated, flowing nanosuspensions, 133 (2019) 205–213.

Bowen, W.R., Gan, Q.J.B., 1991. Properties of microfiltration membranes: flux loss during constant pressure permeation of bovine serum albumin. Bioengineering 38, 688–696.

Brader M.L., Williams S.J., Banks J.M., Hui W.H., Zhou Z.H., Jin L.J.B.j., Encapsulation state of messenger RNA inside lipid nanoparticles, 120 (2021) 2766–2770.

Buetehorn S., Carstensen F., Wintgens T., Melin T., Volmering D., Vossenkaul K.J.D., Permeate flux decline in cross-flow microfiltration at constant pressure, 250 (2010) 985–990.
Cheng, M.H.Y., Leung, J., Zhang, Y., Strong, C., Basha, G., Momeni, A., Chen, Y., Jan, E., Abdolahzadeh, A., Wang, X., 2023a. Induction of bleb structures in lipid nanoparticle formulations of mRNA leads to improved transfection potency. Adv. Mater. 35, 2303370.
Cheng M.H.Y., Leung J., Zhang Y., Strong C., Basha G., Momeni A., Chen Y., Jan E., Abdolahzadeh A., Wang X.J.A.M., Induction of bleb structures in lipid nanoparticle formulations of mRNA leads to improved transfection potency, 35 (2023b) 2303370.
Chheda, U., Pradeepan, S., Esposito, E., Strezsak, S., Fernandez-Delgado, O., Kranz, J., 2024. Factors affecting stability of RNA–temperature, length, concentration, pH, and buffering species. J. Pharm. Sci. 113, 377–385.
Dizon-Maspat, J., Bourret, J., D'Agostini, A., Li, F.J.B., 2012. Single pass tangential flow filtration to debottleneck downstream processing for therapeutic antibody production. Bioengineering 109, 962–970.
Domokos A., Nagy B., Szilagyi B., Marosi G., Nagy Z.K.J.O.P.R., Development, integrated continuous pharmaceutical technologies—A review, 25 (2021) 721–739.
Eckford, C., 2023. First continuous mRNA manufacturing platform to be developed. Eur. Pharm. Rev.
Furukawa K., Judai K.J.T.J.o.C.P., Brownian motion probe for water-ethanol inhomogeneous mixtures, 147 (2017).
Gerstweiler L., Bi J., Middelberg A.P.J.C.E.S., Continuous downstream bioprocessing for intensified manufacture of biopharmaceuticals and antibodies, 231 (2021) 116272.
GY S.J.A.C.E.R., Ethanol and membrane lipids, 185 (1985) 1–5.
Hardianto A., Muscifa Z.S., Widayat W., Yusuf M., Subroto T.J.M., The effect of ethanol on lipid nanoparticle stabilization from a molecular dynamics simulation perspective, 28 (2023) 4836.
Hengelbrock, A., Schmidt, A., Strube, J., 2023. Formulation of nucleic acids by encapsulation in lipid nanoparticles for continuous production of mRNA. Processes 11, 1718.
Highlights of Prescribing Information, 10001, 2021. Manufactured by Pfizer Inc., New York, NY.
I.H.T.J.C.S. Guideline, Impurities: guideline for residual solvents Q3C (R5), 4 (2005) 1–25.
Analytical Procedures for Quality of mRNA Vaccines and Therapeutics, 2023. United States Pharmacopeia.
Jones L.J., Yue S.T., Cheung C.Y., Singer V.L.J.A.B., RNA quantitation by fluorescence-based solution assay: riboGreen reagent characterization, 265 (1998) 368–374.
Kafetzis K.N., Papalamprou N., McNulty E., Thong K.X., Sato Y., Mironov A., Purohit A., Welsby P.J., Harashima H., Yu-Wai-Man C.J.A.H.M., The effect of Cryoprotectants and storage conditions on the transfection efficiency, stability, and safety of lipid-based nanoparticles for mRNA and DNA delivery, 12 (2023) 2203022.
Kauffman K.J., Dorkin J.R., Yang J.H., Heartlein M.W., DeRosa F., Mir F.F., Fenton O.S., Anderson D.G.J.N.L., Optimization of lipid nanoparticle formulations for mRNA delivery *in vivo* with fractional factorial and definitive screening designs, 15 (2015) 7300–7306.
Kim B., Hosn R.R., Remba T., Yun D., Li N., Abraham W., Melo M.B., Cortes M., Li B., Zhang Y.J.J.O.C.R., Optimization of storage conditions for lipid nanoparticle-formulated self-replicating RNA vaccines, 353 (2023) 241–253.
Kimura N., Maeki M., Sato Y., Ishida A., Tani H., Harashima H., Tokeshi M.J.A.A.M., Development of a microfluidic-based post-treatment process for size-controlled lipid nanoparticles and application to siRNA delivery, interfaces, 12 (2020) 34011–34020.
Kimura N., Maeki M., Sato Y., Note Y., Ishida A., Tani H., Harashima H., Tokeshi M.J.A.O., Development of the iLiNP device: fine tuning the lipid nanoparticle size within 10 nm for drug delivery, 3 (2018) 5044–5051.
Kotouček J., Hubatka F., Mašek J., Kulich P., Velínská K., Bezděková J., Fojtíková M., Bartheldyová E., Tomečková A., Stráská J.J.S.R., Preparation of nanoliposomes by microfluidic mixing in herring-bone channel and the role of membrane fluidity in liposomes formation, 10 (2020) 5595.
Lehmann, K., Schmidt, U., 2003. Group II introns: structure and catalytic versatility of large natural ribozymes. Crit. Rev. Biochem. Mol. Biol. 38, 249–303.
Leung A.K., Tam Y.Y.C., Chen S., Hafez I.M., Cullis P.R.J.T.J.O.P.C.B., Microfluidic mixing: a general method for encapsulating macromolecules in lipid nanoparticle systems, 119 (2015) 8698–8706.
Li, Y., Breaker, R.R., 1999. Kinetics of RNA degradation by specific base catalysis of transesterification involving the 2 '-hydroxyl group. J. Am. Chem. Soc. 121, 5364–5372.
Ly H.H., Daniel S., Soriano S.K., Kis Z., Blakney A.K.J.M.P., Optimization of lipid nanoparticles for saRNA expression and cellular activation using a design-of-experiment approach, 19 (2022) 1892–1905.
Malladi S., Coolbaugh M.J., Thomas C., Krishnan S., Varner C.T., Walther J., Brower K.P. J.J.O.M.S., Design of a process development workflow and control strategy for single-pass tangential flow filtration and implementation for integrated and continuous biomanufacturing, 677 (2023) 121633.
Marino K., Levison P.J.G.E., News B., Achieving process intensification with single-pass TFF: improving process economics and speed to market with cross-functional inline concentration, 37 (2017) 30–31.
Maxmen A., The WHO's push for global mRNA vaccine access. Will the WHO hub realize its vision before the next global health crisis?, www.thinkglobalhealth.org., 2024.
Mikkola, S., Lönnberg, T., Lönnberg, H., 2018. Phosphodiester models for cleavage of nucleic acids. Beilstein. J. Org. Chem. 14, 803–837.
Miller D.J., Kasemset S., Paul D.R., Freeman B.D.J.J.O.M.S., Comparison of membrane fouling at constant flux and constant transmembrane pressure conditions, 454 (2014) 505–515.
Moghimi, S.M., Simberg, D., 2022. Pro-inflammatory concerns with lipid nanoparticles. Mol. Ther. 30, 2109–2110.
Nelson, M., 2023. MIT Receives $82m from FDA For Continuous mRNA Manufacturing Platform. BioProcess International.
Qin, S., Tang, X., Chen, Y., Chen, K., Fan, N., Xiao, W., Zheng, Q., Li, G., Teng, Y., Wu, M., 2022. mRNA-based therapeutics: powerful and versatile tools to combat diseases. Signal Transduct. Target. Ther. 7, 166.
Qu J., Nair A., Muir G.W., Loveday K.A., Yang Z., Nourafkan E., Welbourne E.N., Maamra M., Dickman M.J., Kis Z.J.M.T.N.A., Quality by design for mRNA platform purification based on continuous oligo-dT chromatography, 35 (2024).
Reinhart A.G., Osterwald A., Ringler P., Leiser Y., Lauer M.E., Martin R.E., Ullmer C., Schumacher F., Korn C., Keller M.J.M.P., Investigations into mRNA lipid nanoparticles shelf-life stability under nonfrozen conditions, 20 (2023) 6492–6503.
Schoenmaker L., Witzigmann D., Kulkarni J.A., Verbeke R., Kersten G., Jiskoot W., Crommelin D.J.J.I.J.O.P., mRNA-lipid nanoparticle COVID-19 vaccines: Structure and stability, 601 (2021) 120586.
Simonsen, J.B., 2024. A perspective on bleb and empty LNP structures. J. Control. Release 373, 952–961.
Wang, Y.S., Kumari, M., Chen, G.H., Hong, M.H., Yuan, J.P.Y., Tsai, J.L., Wu, H.C., 2023. mRNA-based vaccines and therapeutics: an in-depth survey of current and upcoming clinical applications. J. Biomed. Sci. 30, 84.
Weatherly C.A., Woods R.M., Armstrong D.W.J.J.O.A., f. chemistry, Rapid analysis of ethanol and water in commercial products using ionic liquid capillary gas chromatography with thermal conductivity detection and/or barrier discharge ionization detection, 62 (2014) 1832–1838.
Webb, C., Ip, S., Bathula, N.V., Popova, P., Soriano, S.K., Ly, H.H., Eryilmaz, B., Nguyen Huu, V.A., Broadhead, R., Rabel, M., 2022a. Current status and future perspectives on MRNA drug manufacturing. Mol. Pharm. 19, 1047–1058.
Webb C., Ip S., Bathula N.V., Popova P., Soriano S.K., Ly H.H., Eryilmaz B., Nguyen Huu V.A., Broadhead R., Rabel M.J.M.p., Current status and future perspectives on MRNA drug manufacturing, 19 (2022b) 1047–1058.
Welbourne, E.N., Loveday, K.A., Nair, A., Nourafkan, E., Qu, J., Cook, K., Kis, Z., Dickman, M.J., 2024a. Anion exchange HPLC monitoring of mRNA in vitro transcription reactions to support mRNA manufacturing process development. Front. Mol. Biosci. 11, 1250833.
Welbourne E.N., Loveday K.A., Nair A., Nourafkan E., Qu J., Cook K., Kis Z., Dickman M. J.J.F.I.M.B., Anion exchange HPLC monitoring of mRNA in vitro transcription reactions to support mRNA manufacturing process development, 11 (2024b) 1250833.
Yan L.L., Zaher H.S.J.J.O.B.C., How do cells cope with RNA damage and its consequences?, 294 (2019) 15158–15171.
Zhang, G., Tang, T., Chen, Y., Huang, X., Liang, T., 2023. mRNA vaccines in disease prevention and treatment. Signal Transduct. Target. Ther. 8, 365.